

# Surface-based broadband electromagnetic-circuit simulation of lossy conductors

S. Chakraborty and V. Jandhyala

**Abstract:** Surface-only boundary-element formulations are particularly efficient for electromagnetic modelling of microelectronic structures that consist of homogeneous sections, such as interconnects, packaged and on-chip microwave and analogue circuit components. However, broadband modelling, as necessitated in digital and ultrawideband systems, is not possible with standard surface-only formulations that rely on the surface impedance technique to model conductor loss. In existing methods, recourse is taken to volumetric solvers in such cases. A surface-only formulation is presented that is truly broadband, and solves the internal field problem exactly, utilising a newly developed lossy medium quadrature. The value of the proposed technique lies in its seamless behaviour over wide frequency ranges and its direct interconnectivity to circuit-level analyses. In particular, frequency-dependent parameters can be extracted via a surface-only approach, valid at all frequencies. The electromagnetic analysis is coupled to a lumped circuit formulation, via a recently developed contact model.

## 1 Introduction

Rapid growth in the switching speed, operating frequencies and packing density of integrated digital, analogue, RF and microwave circuits and associated packaging has necessitated the modelling of the EM behaviour of at least parts of the interconnects, passives and substrates of a large circuit. While circuit-level analysis using lumped circuit component models remains valid for substantial sections of the circuit being examined, the distributed 2-D and 3-D components exhibit significant effects on the electrical performance of the microelectronic subsystem. While modelling the entire microelectronic system using a 3-D electromagnetic (EM) solver is impractically expensive, a viable alternative is to use EM simulation on sensitive sections, such as global interconnects, microwave passives components and substrate effects, while the remaining sections are modelled with lumped elements for which standard modified nodal analysis (MNA)-based circuit simulation can be used. The overall simulation then proceeds as a simultaneous, coupled solution that is useful in specific instances such as field-based component placement, or as a circuit-level simulation with EM models replaced by 'port' or equivalent models [1].

Previous work aimed at coupling circuit and EM simulation has been based on finite difference time domain (FDTD) analysis [2]. Incorporation of lumped circuits into FDTD are relatively straightforward. Similar approaches for frequency domain finite difference (FDFD) [3] also exist in EM literature. Finite element techniques (FEM) have also been investigated [4] for coupling EM objects to circuits using port models. In addition to these approaches, it is

desirable to have a coupled circuit-EM approach with integral equations, which are fast becoming the method of choice for interconnect and substrate applications. The partial element equivalent circuit (PEEC) method [5] models the volume of a rectangular interconnect using thin filament basis functions and uses integral equations to substitute the EM-object as a dense network of lumped circuits. Port parameter extraction [1] is another useful step to obtain solutions for circuit-EM problems, where a separate standalone EM solution is performed to extract port parameters. Equivalent circuit models are derived from the port parameters and directly linked to SPICE or other circuit simulators. In circuits where reference grounds are not explicit or obvious, port definitions may be inaccurate or impossible. Postprocessed coupled circuit-EM information relative to the EM part would be more easily accessible in a fully coupled simulation than in a port model. For instance, these effects include ground bounce, hot-spot identification and scattered field computation. Boundary element methods [6] using surface integral formulation have become popular because of their capability of capturing skin effects implicitly. Electromagnetic modelling of microelectronic circuit layouts has been accomplished for perfect electric conductors and also for lossy conducting material at high frequency, where the surface impedance assumption is valid [7–10]. However, for broadband digital applications, volumetric current flow through the conductors can be dominant at lower frequencies, where the skin effect is not valid. Special care needs to be taken in such a situation for modelling the truly volumetric current flow using a surface-only formulation.

The method presented here is focused towards a frequency domain broadband simulation of lossy interconnects and substrates coupled to lumped circuits using surface integral equations and a unified coupling matrix approach. To ensure the generality of solution, to model static, quasistatic and full-wave effects, the full-wave Green's function is used to compute the method of moments (MoM) matrices.

© IEE, 2006

*IEE Proceedings* online no. 20050139

doi:10.1049/ip-map:20050139

Paper first received 10th June and in revised form 20th October 2005

The authors are with the Department of Electrical Engineering, University of Washington, Seattle, WA, 98195, USA

E-mail: swagatoc@yahoo.com

## 2 Electromagnetic formulation

A coupled EM and circuit environment can be decomposed into its constituents as circuit components and EM objects. The EM objects may be in general three-dimensional bodies of arbitrary shape and have material properties defined by finite permeability, permittivity and conductivity. The permittivity can be real or complex depending upon the dielectric loss. The circuit components are included into the system using their standard SPICE models. To specify the relation between the geometry-dependent EM objects, the lumped circuit components and the circuit excitation, it is important to model the behaviour of the EM object under the influence of the circuit components, and vice versa.

For modelling the EM objects, the surface-integral-equation-based method of moments (MoM) technique [11] has been used. The entire problem is decomposed into exterior and interior equivalent problems [12], and the original object is replaced by a mathematical surface, with equivalent electric and magnetic surface currents on the exterior and interior sides of the surface.

For objects with finite conductivity, unlike perfect electric conductors, the tangential electric field does not vanish completely on the surface. Hence, the tangential electric field boundary condition for such objects can be written as

$$\hat{\mathbf{n}}_e \times \mathbf{E}^+ = \hat{\mathbf{n}}_i \times \mathbf{E}^- \neq 0 \quad (1)$$

where  $\hat{\mathbf{n}}_e$  and  $\hat{\mathbf{n}}_i$  are the unit vectors normal to the boundary surface pointing out of and into the conducting region, respectively, ( $\hat{\mathbf{n}}_e = -\hat{\mathbf{n}}_i$ ), and  $\mathbf{E}^+$  and  $\mathbf{E}^-$  are the electric field vectors just outside and inside the conducting region.

Thus, in the equivalent problem, the equivalent surface magnetic current density in the region exterior to the conducting object is given by

$$\mathbf{M}_e = \hat{\mathbf{n}}_e \times \mathbf{E} \neq 0 \quad (2)$$

Similarly, the interior medium surface magnetic current density  $\mathbf{M}_i$ , exterior medium surface electric current density  $\mathbf{J}_e$  and the interior medium surface electric current density  $\mathbf{J}_i$  are given by

$$\mathbf{M}_i = \hat{\mathbf{n}}_i \times \mathbf{E} \quad (3a)$$

$$\mathbf{J}_e = \hat{\mathbf{n}}_e \times \mathbf{H} \quad (3b)$$

$$\mathbf{J}_i = \hat{\mathbf{n}}_i \times \mathbf{H} \quad (3c)$$

For the restricted cases of high-frequency applications, electric current and magnetic current densities are related by the localised impedance boundary condition (IBC) [13], and the equivalent magnetic current density can be eliminated using the following relationship thereby reducing the problem to a single region equivalent electric current only formulation:

$$\mathbf{M} = -Z_S \hat{\mathbf{n}} \times \mathbf{J} \quad (4)$$

where  $Z_S$  is the surface impedance and is given for an angular frequency  $\omega$  by

$$Z_S = (1 + j) \sqrt{\frac{\mu\omega}{2\sigma}} \quad (5)$$

for a region with permeability  $\mu$  and conductivity  $\sigma$ . However, IBC is strictly applicable only at high frequencies, where the skin effect is prominent. The method fails to handle the low-frequency behaviour. It is important to note that for low-frequency behaviour, the issues that arise due to the volumetric nature of the current flow through the conductors, e.g. levelling-off of inductance, resistance, etc. are under focus in the paper. The important but complementary issues of low-frequency conditioning of

the electric field integral equation [14] have not been addressed here.

In order to capture both the low-frequency volumetric effect and the high-frequency skin effect through a single-surface-based methodology, a rigorous two-region PMCHWT formulation is used in this paper to model the electromagnetic behaviour of lossy conductors.

In the two-region formulation, the scattered electric and magnetic fields  $\mathbf{E}^{scat}$  and  $\mathbf{H}^{scat}$  in a region characterised by permeability  $\mu$  and permittivity  $\varepsilon$  are given by

$$\mathbf{E}^{scat} = -j\omega\mathbf{A} - \nabla\phi - \frac{1}{\varepsilon}\nabla \times \mathbf{F} \quad (6a)$$

$$\mathbf{H}^{scat} = \frac{1}{\mu}\nabla \times \mathbf{A} - j\omega\mathbf{F} - \nabla\psi \quad (6b)$$

Where  $\mathbf{A}$ ,  $\mathbf{F}$ ,  $\psi$  and  $\phi$  are the magnetic vector potential, electric vector potential, magnetic scalar potential and electric scalar potential, respectively, and are given by

$$\mathbf{A}(\mathbf{r}) = \frac{\mu}{4\pi} \int_{S'} G(\mathbf{r}, \mathbf{r}') \mathbf{J}(\mathbf{r}') ds' \quad (7a)$$

$$\mathbf{F}(\mathbf{r}) = \frac{\varepsilon}{4\pi} \int_{S'} G(\mathbf{r}, \mathbf{r}') \mathbf{M}(\mathbf{r}') ds' \quad (7b)$$

$$\phi(\mathbf{r}) = \frac{1}{4\pi\varepsilon} \int_{S'} G(\mathbf{r}, \mathbf{r}') \rho(\mathbf{r}') ds' \quad (7c)$$

$$\psi(\mathbf{r}) = \frac{1}{4\pi\mu} \int_{S'} G(\mathbf{r}, \mathbf{r}') \zeta(\mathbf{r}') ds' \quad (7d)$$

$\mathbf{r}$  and  $\mathbf{r}'$  are, respectively, the position of the observation point and the source point,  $S'$  is the source region,  $\rho$ ,  $\zeta$  are the equivalent electric charge density and magnetic charge density on the surface and  $G(\mathbf{r}, \mathbf{r}')$  is the three-dimensional fullwave Green's function in the region where the scattered fields are computed, and is expressed as

$$G(\mathbf{r}, \mathbf{r}') = \frac{e^{-jk|\mathbf{r}-\mathbf{r}'|}}{|\mathbf{r}-\mathbf{r}'|} \quad (8)$$

where  $k$  is the wavenumber for the medium and is given by  $k = \omega\sqrt{\mu\varepsilon}$ . In general, the effective permittivity of a lossy conductor is expressed as

$$\varepsilon_i = \varepsilon_0\varepsilon_r \left( 1 + \frac{\sigma}{j\omega\varepsilon_0} \right) \quad (9)$$

where  $\varepsilon_0$ ,  $\varepsilon_r$  and  $\sigma$  are the free-space permittivity, the relative dielectric constant and the conductivity of the material, respectively. For a conducting material the wavenumber is a complex quantity given by

$$k = \omega\sqrt{\mu\varepsilon_0 \left( 1 + \frac{\sigma}{j\omega\varepsilon_0} \right)} \quad (10)$$

Finally, the tangential boundary condition is written on the field quantities across the interface as

$$\mathbf{E}_e^{scat}|_{tan} + \mathbf{E}_e^{exc}|_{tan} = \mathbf{E}_i^{scat}|_{tan} + \mathbf{E}_i^{exc}|_{tan} \quad (11a)$$

$$\mathbf{H}_e^{scat}|_{tan} + \mathbf{H}_e^{exc}|_{tan} = \mathbf{H}_i^{scat}|_{tan} + \mathbf{H}_i^{exc}|_{tan} \quad (11b)$$

Where  $\mathbf{E}_e^{exc}$ ,  $\mathbf{E}_i^{exc}$ ,  $\mathbf{H}_e^{exc}$  and  $\mathbf{H}_i^{exc}$  are the electric and magnetic field excitations in the exterior and the interior regions, respectively, and the suffix *tan* denotes the field component tangential to the surface. From (6) and (11)

$$\begin{aligned} & \left( -j\omega\mathbf{A}_e - \nabla\phi_e - \frac{1}{\varepsilon_e}\nabla \times \mathbf{F}_e + \mathbf{E}_e^{exc} \right)_{tan} \\ & = \left( -j\omega\mathbf{A}_i - \nabla\phi_i - \frac{1}{\varepsilon_i}\nabla \times \mathbf{F}_i + \mathbf{E}_i^{exc} \right)_{tan} \end{aligned} \quad (12a)$$

$$\begin{aligned} & \left( \frac{1}{\mu} \nabla \times \mathbf{A}_e - j\omega \mathbf{F}_e - \nabla \psi_e + \mathbf{H}_e^{exc} \right)_{tan} \\ & = \left( \frac{1}{\mu} \nabla \times \mathbf{A}_i - j\omega \mathbf{F}_i - \nabla \psi_i + \mathbf{H}_i^{exc} \right)_{tan} \end{aligned} \quad (12b)$$

In the MoM formulation, the electric and magnetic source currents are expanded using the triangular-pair-based Rao–Wilton–Glisson (RWG) basis functions [11]. For the exterior region, the Green's function convolutions over the triangular source regions are carried out using the standard singularity extraction and analytic technique [15]. However, if the interior medium is highly conducting, then the Green's function, even after extracting the  $1/|\mathbf{r} - \mathbf{r}'|$  singularity would exhibit a very fast spatially decaying nature. In such a situation, the standard 2-D Gaussian quadrature rules are insufficient to capture the functional decay, and adaptive polar-co-ordinate-based analytic integration rules [16] are required.

### 3 Circuit coupling

In order to analyse the effect of attaching lumped circuit components to a conducting structure, whose surface is given by  $S$ , the surface  $S$  (Fig. 1) is divided into two subsurfaces, as described in a recently developed contact model [9] for coupled circuit and electromagnetic simulation. The subsurfaces are denoted by  $S_{CK}$  and  $S_{EM}$  such that

$$S_{EM} \cup S_{CK} = S \quad (13a)$$

and

$$S_{EM} \cap S_{CK} = \Phi \quad (13b)$$

$S_{CK}$  is the portion of  $S$  that is attached to the lumped circuit elements and  $S_{EM}$  is the remaining portion of  $S$  that supports equivalent surface currents modelled using RWG basis functions. On  $S_{EM}$  the equivalent surface electric current density is related to the equivalent surface electric charge density through the standard continuity equation, on both the exterior medium and the interior medium.

$$\nabla_S \cdot \mathbf{J}_l(\mathbf{r}) + j\omega \rho_l(\mathbf{r}) = 0, \quad \forall \mathbf{r} \in S_{EM} \quad (14a)$$

$$\rho_l(\mathbf{r}) = \frac{-\nabla_S \cdot \mathbf{J}_l(\mathbf{r})}{j\omega} \quad \forall \mathbf{r} \in S_{EM} \quad (14b)$$

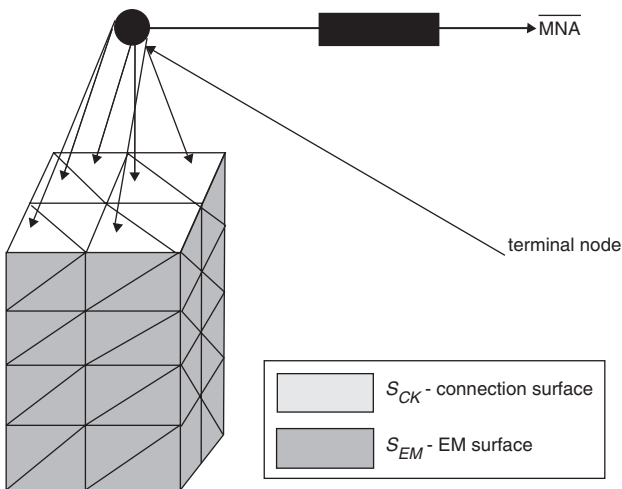


**Fig. 1** Electromagnetic surface and connection surface on an object

where  $\nabla_S$  represents surface divergence, and  $l$  can be either  $e$  or  $i$  depending upon whether the equation is written for the exterior or the interior medium. Similarly, equivalent surface magnetic current density is related to the equivalent surface magnetic charge density for the entire surface  $S$  through the continuity equation as

$$\nabla_S \cdot \mathbf{M}_l(\mathbf{r}) + j\omega \zeta_l(\mathbf{r}) = 0, \quad \forall \mathbf{r} \in S_{EM} \cup S_{CK} \quad (15a)$$

$$\zeta_l(\mathbf{r}) = \frac{-\nabla_S \cdot \mathbf{M}_l(\mathbf{r})}{j\omega} \quad \forall \mathbf{r} \in S_{EM} \cup S_{CK} \quad (15b)$$

The relation between the surface electric charge density and the surface electric current density for the connection surface  $S_{CK}$  is obtained by writing the Kirchoff's current law involving the circuit currents and the equivalent surface currents.

Let the  $m$ th triangle on the tessellation of  $S_{CK}$  be given by  $S_{CK}^m$ ,  $m = 1, 2, \dots, N_{pc}$ , where  $N_{pc}$  is the total number of such triangles on  $S_{CK}$ . On triangle  $S_{CK}^m$  the modified continuity equation has the following form for the exterior and the interior medium:

$$\nabla_S \cdot \mathbf{J}_l(\mathbf{r}_m) + j\omega \rho_l(\mathbf{r}_m) = \frac{I_c^m}{A_m}, \quad \forall \mathbf{r} \in S_{CK} \quad (16a)$$

$$\rho_l(\mathbf{r}_m) = \frac{-\nabla_S \cdot \mathbf{J}_l(\mathbf{r}_m)}{j\omega} + \frac{I_c^m}{j\omega A_m} \quad \forall \mathbf{r} \in S_{CK}, \quad m \in \{1, 2, \dots, N_{pc}\} \quad (16b)$$

Here,  $I_c^m$  is the true circuit current that impinges upon the EM object through the triangle  $S_{CK}^m$  and  $A_m$  is the area of the triangle. The circuit current contributes to both the exterior and the interior medium in a similar way as an additional surface charge source; the electric field due to these additional charge-sources act as the excitation for the EM system in conjunction with any EM field excitation that might be present.

The reverse coupling, specifying the effect of the EM current on the circuit quantities, is modelled by matching electric scalar potential on triangle  $S_{CK}^m$  with the voltage of the circuit node it connects to. Equation (7c) can be written for the exterior medium problem for computing the electric scalar potential on the connection triangles as

$$\phi_m(\mathbf{r}_m) = \frac{1}{4\pi\epsilon_e} \sum_{i=1}^{N_e} \int_{S_i'} G_e(\mathbf{r}_m, \mathbf{r}_i') \rho_e(\mathbf{r}_i') ds' \quad \mathbf{r}_m \in S_{CK}, \quad \mathbf{r}_i' \in S_{EM} \cup S_{CK} \quad (17)$$

The electrical potential of a circuit node connected to the EM object through a set of connection triangles  $S_{CK}^m$  is enforced to be equal to the electric scalar potential computed from (17) on the triangles  $S_{CK}^m$ . Every group of triangles that are located contiguously and connected to one circuit node forms one terminal. Since these terminals do not require the presence of a reference ground, they are more general and more flexible than classical port models.

## 4 Coupled EM-circuit matrix system

The coupled EM-circuit problem is solved by a single system of linear equations. The coupled matrix is composed by assembling three parts, namely the EM block, the circuit block and the connection block.

### 4.1 EM block

The EM block represents the contribution of the RWG current [11] unknowns towards the equations enforcing the tangential continuity of  $\mathbf{E}$  and  $\mathbf{H}$  fields across the lossy conductor boundary. The electric scalar potential in this

part of the matrix has contribution only from the divergence of the surface electric current in the interior and the exterior medium, i.e. only the first term of the right-hand side of (16b). In summary, the EM block can be written as a regular two-region PMCHWT matrix [12] as

$$j\omega \langle (\mathbf{A}_e - \mathbf{A}_i), \mathbf{t} \rangle + \left\langle \left( \vec{\nabla} \tilde{\phi}_e - \vec{\nabla} \tilde{\phi}_i \right), \mathbf{t} \right\rangle + \left\langle \vec{\nabla} \times \left( \frac{\mathbf{F}_e}{\varepsilon_e} - \frac{\mathbf{F}_i}{\varepsilon_i} \right), \mathbf{t} \right\rangle = \langle (\mathbf{E}_e^{Exc} - \mathbf{E}_i^{Exc}), \mathbf{t} \rangle \quad (18a)$$

$$- \left\langle \vec{\nabla} \times \left( \frac{\mathbf{A}_e}{\mu_e} - \frac{\mathbf{A}_i}{\mu_i} \right), \mathbf{t} \right\rangle + j\omega \langle (\mathbf{F}_e - \mathbf{F}_i), \mathbf{t} \rangle + \left\langle \left( \vec{\nabla} \psi_e - \vec{\nabla} \psi_i \right), \mathbf{t} \right\rangle = \langle (\mathbf{H}_e^{Exc} - \mathbf{H}_i^{Exc}), \mathbf{t} \rangle \quad (18b)$$

where  $\mathbf{t}$  is the testing function, which in this case is the same as the RWG basis functions (Galerkin testing [11]) and  $\tilde{\phi}_e, \tilde{\phi}_i$  are the electric scalar potential in the exterior and interior medium only due to the divergence of the surface electric current. The potential terms can be computed using (7a)–(7d) as a function of the equivalent surface electric and magnetic current in the exterior and the interior media. In assembling the PMCHWT matrix, it is possible to reuse the integrals  $\mathbf{A}$  and  $\phi$  to obtain  $\mathbf{F}$  and  $\psi$  with appropriate scaling and sign. Equation (18) forms a  $2N_e \times 2N_e$  MoM matrix  $\bar{\mathbf{E}}_{11}$ , where  $N_e$  is the number of surface triangle edges on  $S$ .

#### 4.2 Circuit block

The circuit part represents Kirchoff's current law and Kirchoff's voltage law for the circuit nodes and circuit branches. The circuit block is obtained by the standard modified nodal analysis (MNA) technique [17] by assembling the individual stamps for the elements. Details of the MNA method is standard in literature and has been omitted from this paper.

#### 4.3 Connection blocks

The EM block and the circuit block do not have any direct coupling, but they are coupled through the connection blocks. There are five connection blocks, namely  $\bar{\mathbf{E}}_{12}$ ,  $\bar{\mathbf{E}}_{21}$ ,  $\bar{\mathbf{E}}_{22}$ ,  $\bar{\mathbf{C}}_1$  and  $\bar{\mathbf{C}}_2$ .

As described in (16), the total surface charge for the connection triangles  $S_{CK}$  consists of two separate terms, of which only one term is already included in (18a). The remaining term, i.e. contribution from the additional surface charge due to the circuit current, is modelled as an extra source term giving rise to additional electric scalar potential  $\phi'_i$  in both the media as

$$\phi'_i(\mathbf{r}) = \frac{1}{4\pi\varepsilon_l} \sum_{m=1}^{N_{pc}} \int_{S_{CK}^m} \frac{I_c^m e^{-jk_l |\mathbf{r} - \mathbf{r}_c^m|}}{j\omega A_m |\mathbf{r} - \mathbf{r}_c^m|} ds_{ck} \quad (19)$$

This potential contributes to a tested electric field in addition to the electric scalar potential contribution  $\tilde{\phi}_l$  in (18). This contribution gives rise to a rectangular matrix block  $\bar{\mathbf{E}}_{12}$  of size  $N_e \times N_{pc}$ , where  $N_{pc}$  is the number of connection triangles.

Equation (17) describes the coupling equation enforcing the circuit node potential to be equal to the electric scalar potentials at the connection triangles due to the divergence of the equivalent surface electric current and the additional source-charge arising from the circuit current. This equation is written as two separate terms

$$\phi_{CK}^m(\mathbf{r}) = \tilde{\phi}_{CK}^m(\mathbf{r}) + \phi'_{CK}^m(\mathbf{r}), \quad m = \{1, 2 \dots N_{pc}\} \quad (20)$$

where the contribution from the equivalent electric surface current is

$$\tilde{\phi}_{CK}^m(\mathbf{r}_m) = \frac{-1}{4\pi j\omega\varepsilon_e} \sum_{i=1}^{N_e} \int \frac{\vec{\nabla} \cdot \mathbf{J}_e(\mathbf{r}'_i) e^{-jk_e |\mathbf{r}_m - \mathbf{r}'_i|}}{|\mathbf{r}_m - \mathbf{r}'_i|} ds_{EM} \quad (21)$$

and that of the circuit current is

$$\phi'_{CK}^m(\mathbf{r}_m) = \frac{1}{4\pi j\omega\varepsilon_e} \sum_{i=1}^{N_{pc}} \frac{I_c^i}{A_i} \int \frac{e^{-jk_e |\mathbf{r}_m - \mathbf{r}'_i|}}{|\mathbf{r}_m - \mathbf{r}'_i|} ds_{CK} \quad (22)$$

Equation (21) is written as a rectangular matrix block  $\bar{\mathbf{E}}_{21}$ , of size  $N_{pc} \times N_e$ , and (22) results in a square matrix block  $\bar{\mathbf{E}}_{22}$  of size  $N_{pc} \times N_{pc}$ .

Additionally, the sparse rectangular matrix block  $\bar{\mathbf{C}}_1$  of size  $N_{pc} \times N_c$ , where  $N_c$  is the number of circuit unknowns, enforces the potentials of the circuit nodes that are connected to the EM object to be equal to scalar potential of the corresponding EM connection triangle as defined by (20). Also, another rectangular sparse matrix block  $\bar{\mathbf{C}}_2$  of size  $N_c \times N_{pc}$  enforces the Kirchoff's current law on the node where circuit currents are branched to become the currents coming onto the contact patches of the EM objects.

#### 4.4 Matrix

The matrix corresponds to a system of linear equations which is of size  $(2N_e + N_{pc} + N_c) \times (2N_e + N_{pc} + N_c)$ , where the first  $N_e$  equations are the EM equations enforcing the boundary condition onto the electric field and the next  $N_e$  are similar ones for the magnetic field. Of the remaining  $N_{pc} + N_c$  equations, the first  $N_{pc}$  are the coupling equations to enforce the equality of the electric scalar potential at the contact patches with the corresponding circuit node voltages, and the last  $N_c$  equations are the circuit equations corresponding to the modified nodal analysis.

Similarly, the first  $N_e$  unknowns are the equivalent surface electric current and the next  $N_e$  are the equivalent surface magnetic current. Together these first  $2N_e$  unknowns are the EM unknowns as described in Section 4.1. Of the last  $N_{pc} + N_c$  unknowns, the first  $N_{pc}$  are the connection unknowns that represent the circuit currents entering contact patches as described in Section 4.3. Finally, the last  $N_c$  are the circuit unknowns describing the branch currents in the associated lumped circuit as described in Section 4.2. The overall system of equations is shown in Fig. 2 in matrix form.

$\bar{\mathbf{E}}_J$  and  $\bar{\mathbf{E}}_M$  are the tested scattered electric field matrices from the electric and magnetic surface current sources as given in (18a). Similarly,  $\bar{\mathbf{H}}_J$  and  $\bar{\mathbf{H}}_M$  are the tested scattered magnetic field matrices from the electric and

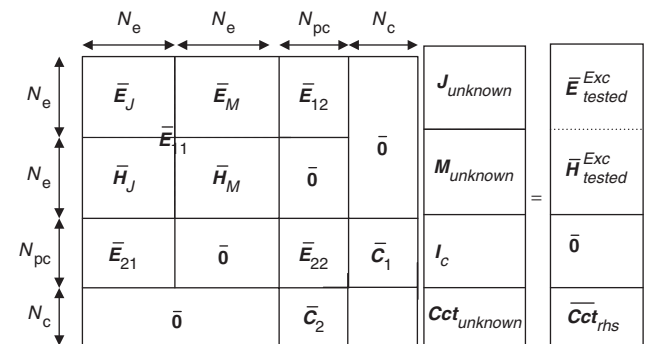


Fig. 2 Overall system of equations

magnetic surface currents, as in (18b). These four blocks together form the  $\overline{\mathbf{E}}_{11}$  matrix.  $\overline{\mathbf{E}}_{12}$ ,  $\overline{\mathbf{E}}_{21}$  and  $\overline{\mathbf{E}}_{22}$  matrices correspond to (15), (21) and (22), respectively.  $\overline{\mathbf{C}}_1$  and  $\overline{\mathbf{C}}_2$  are sparse topological matrices with  $\overline{\mathbf{C}}_2 = \overline{\mathbf{C}}_1^T$ .  $\mathbf{MNA}$  is the modified nodal analysis matrix for the circuit excitation. In the right-hand side vector,  $\mathbf{E}_{tested}^{Exc}$  and  $\mathbf{H}_{tested}^{Exc}$  are the tested electric field and magnetic field excitation, in addition to the lumped circuit excitations.  $\mathbf{Cct}_{rhs}$  corresponds to the independent voltage or current source in the circuit.

#### 4.5 Volumetric current flow

The proposed method exploits the surface equivalence principle to model the EM problem using an equivalent surface current instead of volumetric currents, thus reducing the number of unknown basis functions. However, it is possible to obtain the actual volumetric current through the cross-section of the conductor as a postprocessing step. The volumetric current  $\mathbf{J}_{vol}$  is related to the electric field  $\mathbf{E}_{int}$  at a given point inside the conductor by

$$\mathbf{J}_{vol} = \sigma \mathbf{E}_{int} \quad (23)$$

where the interior electric field is given by

$$\mathbf{E}_{int} = -j\omega \mathbf{A}(\mathbf{J}_i) - \nabla \phi \left( \frac{\nabla \cdot \mathbf{J}_i}{-j\omega} \right) - \nabla \phi \left( \frac{I_c}{-j\omega} \right) \quad (24)$$

## 5 Numerical results

This Section discusses the numerical simulation results obtained by incorporating the proposed methodology in a field solver. Broadband inductance and resistance of a conducting bar of dimension  $0.5 \text{ mm} \times 0.5 \text{ mm} \times 5 \text{ mm}$  and conductivity  $5.8 \times 10^7 \text{ S m}^{-1}$ , i.e. that of copper, are extracted using a coupled circuit-EM simulation. The conductor is modelled using 388 surface triangles. There are 1164 unknowns, including the unknown coefficients of the equivalent surface electric and magnetic current. The simulation takes 22.1 Mbytes of computer memory, 40 s of setup time and 34 s of solution time using LU decomposition in a 2.99 GHz Pentium 4 personal computer. The simulated inductance exhibits (Fig. 3a) expected behaviour, including levelling-off at low frequency and high frequency. The steady inductance values at low frequency and high frequency (100 MHz) are compared against the values obtained from a commercial solver, Ansoft Si3D. Ansoft Si3D uses a magnetostatic volumetric formulation and a surface-impedance-based model for low and high frequencies, respectively. For simple structures like a single bar, the quasistatic resistance can be computed analytically from the skin depth at a given frequency. The analytic value of the resistance exhibits (Fig. 3b) closely match the simulation result, including the low-frequency level-off. Inductance and resistance behaviours are also obtained from a separate quasistatic solver, where the loss is modelled using surface impedance. For higher frequencies, the surface impedance results match the PMCHWT results and also the results from the commercial solver. However, for lower frequencies, the surface-impedance-based model fails to capture the level-off of the resistance and the inductance curves that arise due to uniform current flow through the conductor cross-section. Figure 4 demonstrates the effect of the radiation resistance captured by a fullwave simulation at higher frequencies.

In Fig. 5, two high aspect ratio interconnects are placed next to each other and the coupled simulation is carried out to obtain the self and mutual resistances and inductances at both high and low frequencies (Table 1). The interconnects

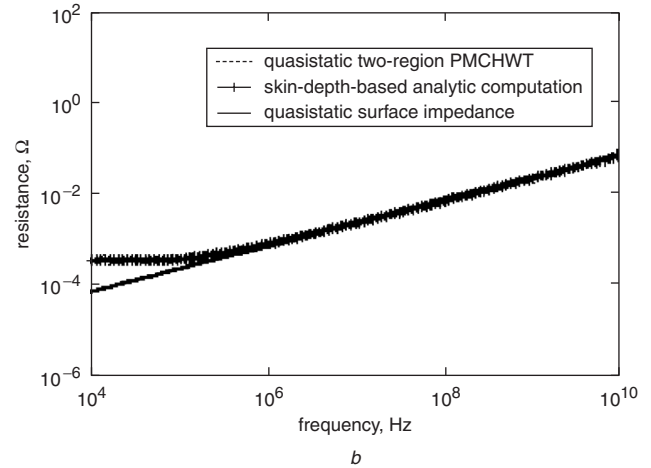
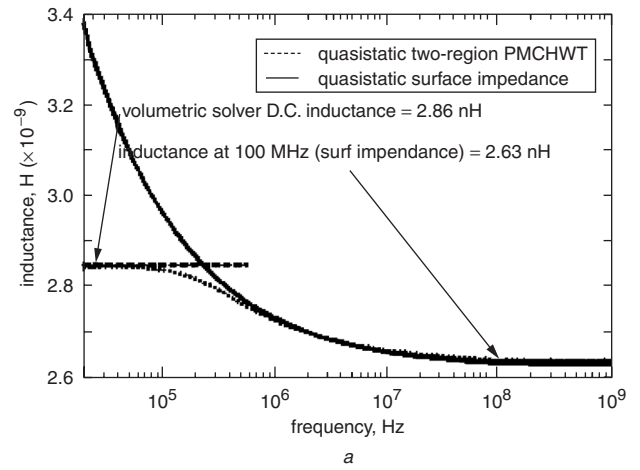


**Fig. 3** Inductance and resistance of a  $0.5 \text{ mm} \times 0.5 \text{ mm} \times 5 \text{ mm}$  copper bar

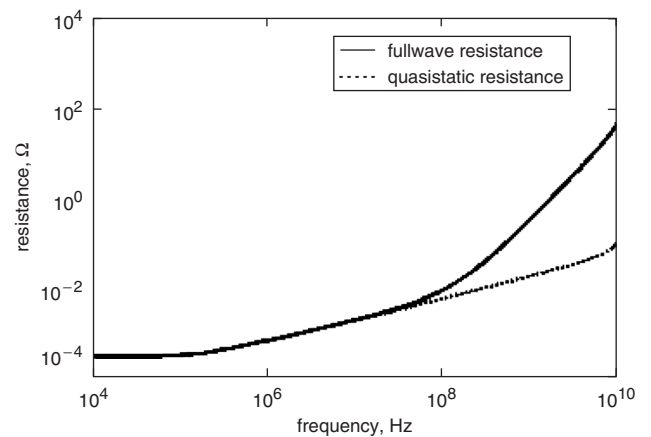


**Fig. 4** Fullwave model for the radiation resistance of a  $0.5 \text{ mm} \times 0.5 \text{ mm} \times 5 \text{ mm}$  copper bar

are modelled using 832 surface triangles resulting in 2496 unknowns. The simulation uses 99 Mbytes of computer memory, 138 s to set up and 108 s to solve using a 2.99 GHz Pentium 4 personal computer. The simulation results are in good agreement with those obtained from Ansoft Si3D. Figure 5 shows the surface current distribution at higher frequencies, where due to the skin effect, most of the current flows closer to the upper and lower surfaces of the conductor (due to high aspect ratio).

**Table 1: Self and mutual resistance and inductance of two parallel traces, extracted using the Ansoft Si3D solver, and a solver based on the methodology presented in the paper**

	1 MHz				100 MHz			
	$R_{11}$ , m $\Omega$	$R_{12}$ , m $\Omega$	$L_{11}$ , nH	$L_{12}$ , nH	$R_{11}$ , m $\Omega$	$R_{12}$ , m $\Omega$	$L_{11}$ , nH	$L_{12}$ , nH
Ansoft Si3D	0.229	0	4.47	2.92	7.68	$-1 \times 10^{-2}$	3.99	2.86
Our method	0.22	$-4 \times 10^{-3}$	4.33	2.92	7.71	$-2 \times 10^{-2}$	4.0	2.86
Difference	4%	-	3%	0%	0.3%	50%	0.2%	0%

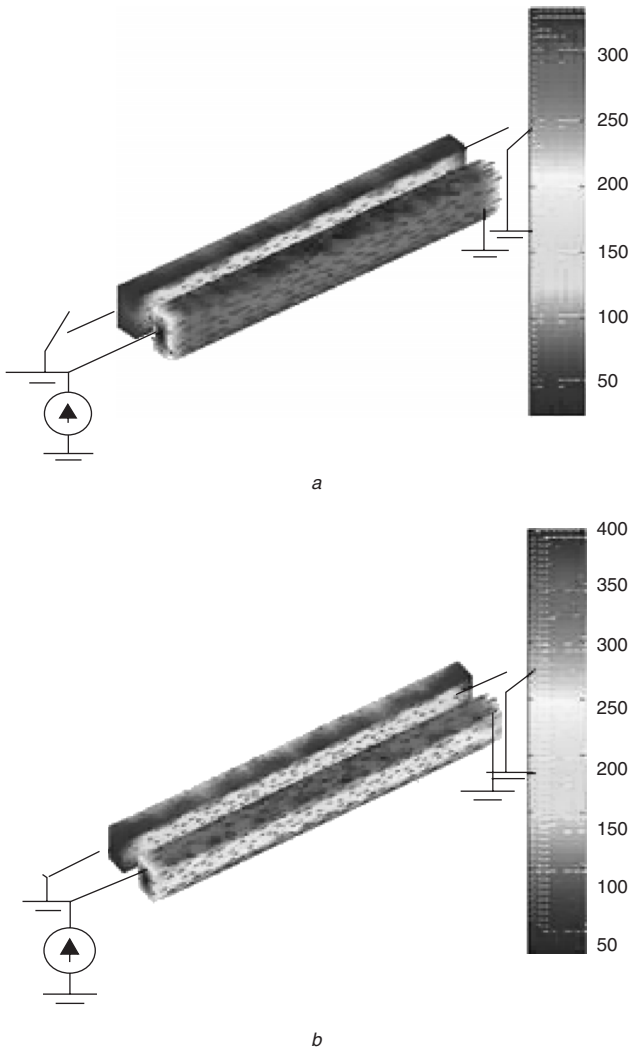


**Fig. 5** Two parallel copper traces with dimensions  $8 \times 0.5 \times 1.2$  mm each, separated by 0.5 mm  
 a 1 MHz  
 b 100 MHz  
 (current density in amps per metre)

Table 2 compares the resistance and inductance of a 3-D spiral inductor with a conductivity of  $5.8 \times 10^4 \text{ Sm}^{-1}$  at 1 MHz and a conductivity of  $5.8 \times 10^7 \text{ Sm}^{-1}$  at 100 MHz with Ansoft Si3D results. The spiral inductor is modelled using 1146 surface triangles resulting in 3438 unknowns. The simulation uses 190.3 Mbytes of memory, 344 s to set up the MoM matrix and 470 s to solve the matrix by the LU decomposition method using a 2.99 GHz Pentium 4 personal computer. In both cases the simulated resistance and inductance match well with the commercial solver. It is important to note that the commercial solver uses the magnetostatic formulation for low-frequency analysis and the surface impedance technique for high-frequency

**Table 2: Resistance and inductance of the coil, computed by the Ansoft Si3D solver, and the solver based on the methodology presented in the paper**

	$\sigma = 5.8 \times 10^4 \text{ Sm}^{-1}$ , $f = 1 \text{ MHz}$		$\sigma = 5.8 \times 10^7 \text{ Sm}^{-1}$ , $f = 100 \text{ MHz}$	
	$R$ , $\Omega$	$L$ , H	$R$ , $\Omega$	$L$ , H
Ansoft Si3D	0.4672	$11.8 \times 10^{-9}$	0.0285	$9.2 \times 10^{-9}$
Proposed method	0.4666	$11.9 \times 10^{-9}$	0.0286	$9.3 \times 10^{-9}$
Difference	0.1%	0.8%	0.3%	1.0%

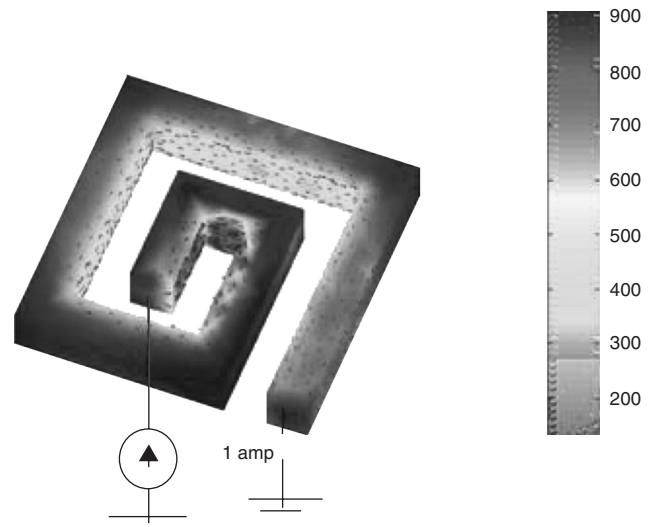


**Fig. 6** Current distribution in a coil  
 Frequency 100 MHz, conductivity  $5.8 \times 10^7 \text{ Sm}^{-1}$

analysis, whereas the presented formulation uses the same formulation in the entire frequency range seamlessly. Figure 6 shows the equivalent surface current distribution on the spiral inductor at 100 MHz, where the current tends to flow in a smaller loop in order to minimise the loop inductance.

Volumetric current flow through the conductor as obtained from (21)–(23) is plotted for conductors with different conductivities in Fig. 7. At low conductivity (Fig. 7a), the current flow is uniform in the cross-section. Increasing conductivity reduces the skin depth, and more current flows near the edges crowding particularly at the corners (Figs. 7b–7d). However, the total current flow when integrated over the entire cross-section is always constant and equal to the total circuit current pushed into the conductor by the circuit. Variation of the current density in the cross-section of the bar is observed (Fig. 8) to have the same decay as that obtained analytically by skin-depth computation.

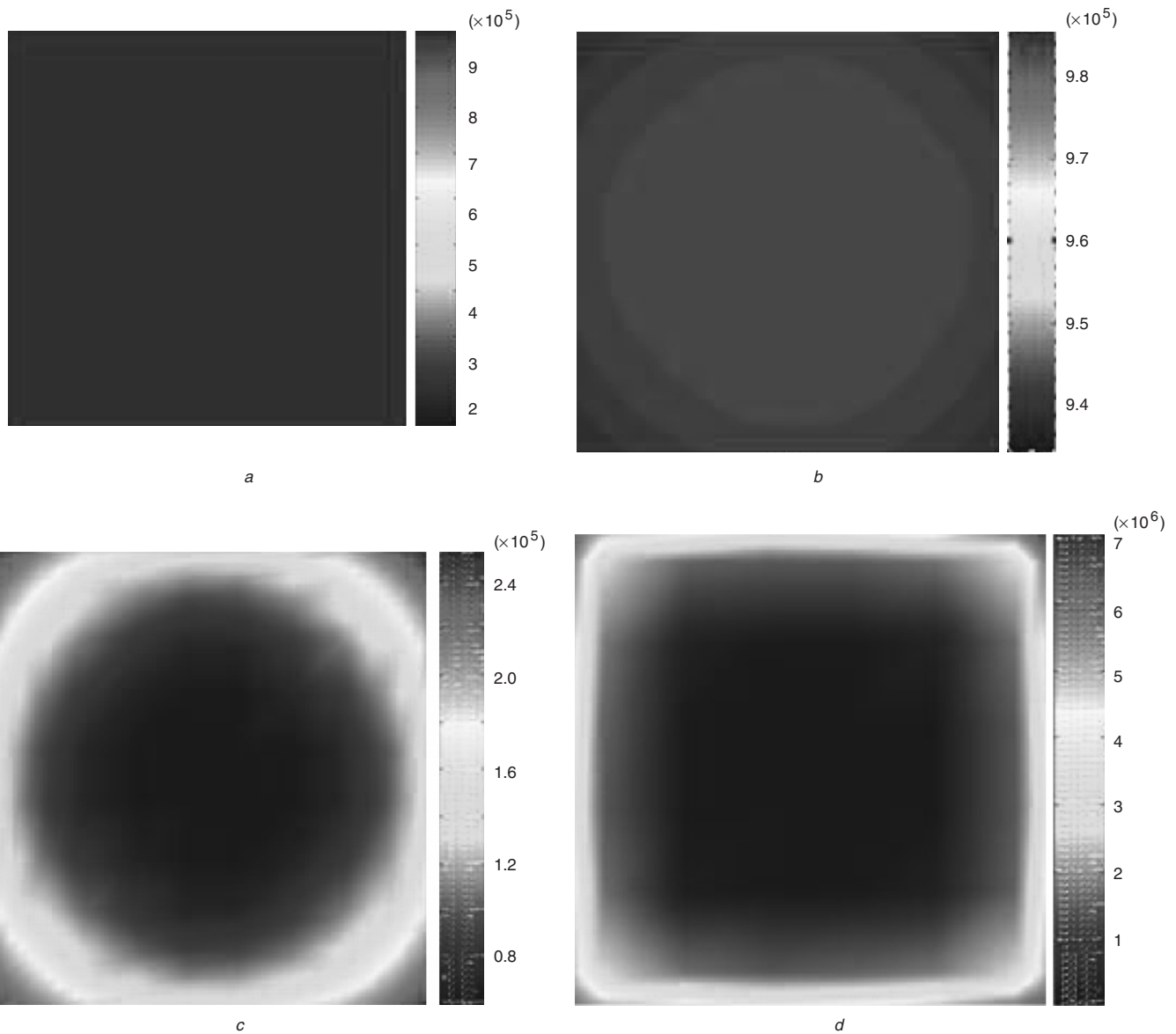


**Fig. 7** Current distribution in the cross-section of a square conductor  
*a*  $J_{min}/J_{max} = 0.99$ , frequency = 1 MHz,  $\sigma = 5.8 \times 10^4$   
*b*  $J_{min}/J_{max} = 0.52$ , frequency = 1 MHz,  $\sigma = 5.8 \times 10^5$   
*c*  $J_{min}/J_{max} = 0.1037$ , frequency = 1 MHz,  $\sigma = 5.8 \times 10^6$   
*d*  $J_{min}/J_{max} = 0.0009$ , frequency = 1 MHz,  $\sigma = 5.8 \times 10^7$

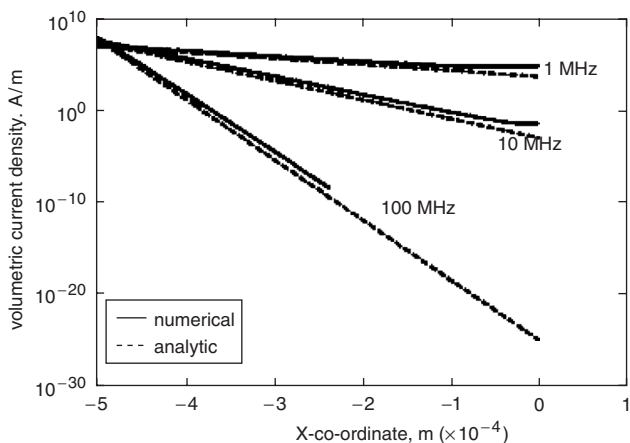


**Fig. 8** Variation of volumetric current density with the distance from the surface ( $x = -0.5$  mm) of a copper conductor with uniform cross-section of  $1$  mm  $\times$   $1$  mm

The proposed methodology can also be used to characterise the bulk current flow through the substrate.

In Fig. 9, 1 mA current is injected into a substrate of dimension  $250 \mu\text{m} \times 250 \mu\text{m} \times 50 \mu\text{m}$ , with relative permittivity of 11.9 and conductivity of  $10 \text{ Sm}^{-1}$ , and there are two other contact points through which the current is taken out. In Fig. 9*a* the contact nearer to the source has higher load impedance, so more current flows through the one further from the source in order to minimise the loss in the total path. Whereas in Fig. 9*b*, the two output contacts have the same load impedance and more current flows through the contact nearer to the input to minimise the substrate loss.

## 6 Conclusions

A novel broadband surface-only methodology is presented for modelling lossy conductors in the presence of lumped

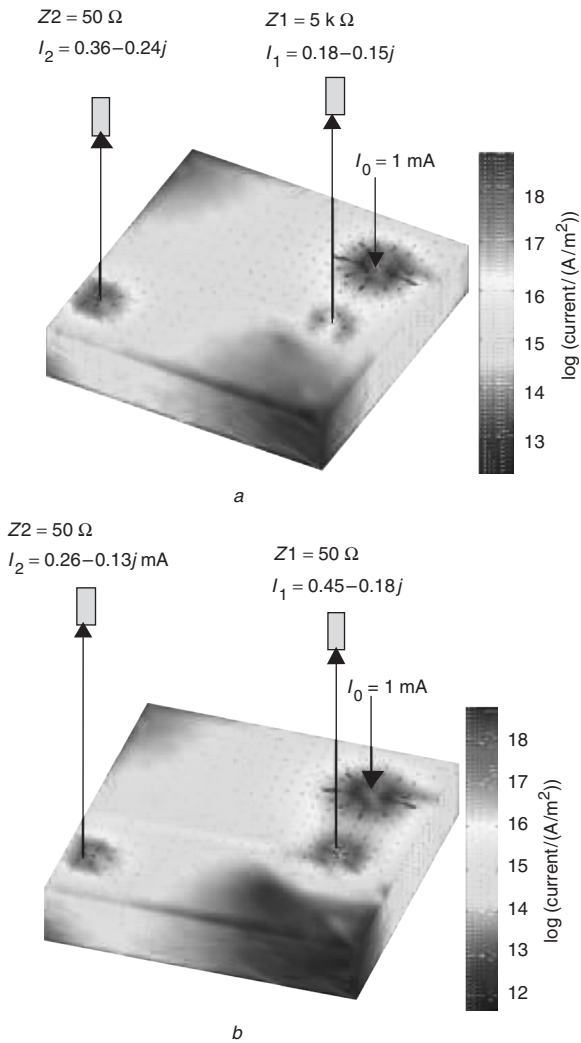


**Fig. 9** Volumetric current distribution with current injection in a substrate where the output points are terminated  
 a Unequal load  
 b Equal load

circuit elements. The method is applicable to microelectronic substrate and interconnect simulation. The presented methodology has been validated against commercial solvers and analytic results.

## 7 Acknowledgments

This work was supported in part by DARPA-MTO NeoCAD grant N66001-01-1-8920. The authors would also like to acknowledge Drs. Y. Wang and D. Gope for their support with the numerical simulations.

## 8 References

- 1 Odabasioglu, A., Celik, M., and Pileggi, L.: 'PRIMA: passive reduced-order interconnect macromodelling algorithm', *IEEE Trans. Comput.-Aided Des. Integr. Circuits Syst.*, 1998, **17**, (8), pp. 645–654
- 2 Taflove, A.: 'Computational electrodynamics: the finite-difference time-domain method' (Artech House, Boston, 1995)
- 3 Haffa, S., Hollmann, D., and Wiesbeck, W.: 'The finite difference method for S-parameter calculation of arbitrary three-dimensional structures', *IEEE Trans. Microw. Theory Tech.*, 1992, **40**, (8), pp. 1602–1610
- 4 Jin, J.: 'The finite element method in electromagnetics' (John Wiley & Sons, New York, 1993)
- 5 Ruehli, A.: 'Equivalent circuit models for three-dimensional multi-conductor systems', *IEEE Trans. Microw. Theory Tech.*, 1974, **22**, (3), pp. 216–221
- 6 Wang, J., Tausch, J., and White, J.: 'A wide frequency range surface integral formulation for 3-D RLC extraction'. Digest of Technical Papers Int. Conf. on Computer-aided Design, 1999, pp. 453–457
- 7 Rong, A., and Cangellaris, A.C.: 'Generalized PEEC models for three-dimensional interconnect structures and integrated passives of arbitrary shapes'. Proc. Topical Meeting on Electrical Performance of Electronic Packaging, 2001, pp. 225–228
- 8 Ponnappalli, S., Bertin, R., and Deutsch, A.: 'A package analysis tool based on a method of moments/surface formulation'. Proc. 43rd Electronic Components and Technology Conf., 1993, pp. 615–622
- 9 Yong, W., Gope, D., Jandhyala, V., and Shi, R.: 'Generalized Kirchoff's current and voltage law formulation for coupled circuit-electromagnetic simulation with surface integral equations', *IEEE Trans. Microw. Theory Tech.*, 2004, **52**, (7), pp. 1673–1682
- 10 van Deventer, T.E., Katehi, L.P., and Cangellaris, A.C.: 'Analysis of conductor losses in high-speed interconnects', *IEEE Trans. Microw. Theory Tech.*, 1994, **42**, (1), pp. 78–83
- 11 Rao, S.M., Wilton, D.R., and Glisson, A.W.: 'Electromagnetic scattering by surfaces of arbitrary shape', *IEEE Trans. Antennas Propag.*, 1982, **30**, (3), pp. 409–418
- 12 Umashankar, K., Taflove, A., and Rao, S.: 'Electromagnetic scattering by arbitrarily shaped three-dimensional homogeneous lossy dielectric objects', *IEEE Trans. Antennas Propag.*, 1986, **34**, (6), pp. 758–766
- 13 Glisson, A.W.: 'Electromagnetic scattering by arbitrarily shaped surfaces with impedance boundary conditions', *Radio Sci.*, 1992, **27**, (6), pp. 935–943
- 14 Chen, S., Zhao, J.S., and Chew, W.C.: 'Analyzing low-frequency electromagnetic scattering from a composite object', *IEEE Trans. Geosci. Remote Sens.*, 2002, **40**, (2), pp. 426–433
- 15 Wilton, D.R., Rao, S.M., Glisson, A.W., Schaubert, D.H., Al-Bundak, O.M., and Butler, C.M.: 'Potential integrals for uniform and linear source distributions on polygonal and polyhedral domain', *IEEE Trans. Antennas Propag.*, 1984, **32**, pp. 276–281
- 16 Chakraborty, S., and Jandhyala, V.: 'Evaluation of Green's function integrals in conducting media'. Proc. IEEE Antennas and Propagation Symp., 23–26 June 2003, pp. 320–323
- 17 Chung-Wen, H., Ruehli, A., and Brennan, P.: 'The modified nodal approach to network analysis', *IEEE Trans. Circuits Syst.*, 1975, **22**, (6), pp. 504–509